ChemSusChem

Research Article
doi.org/10.1002/cssc.202501564

Chemistry Europe
European Chemical Societies Publishing

www.chemsuschem.org

Core and End-Capped Engineering as a Powerful Tool in the Search of Long-Term High-Performance Dye-Sensitized Solar Cells

Matías J. Alonso-Navarro, Santiago Franco,* Fátima Suárez-Blas, Raquel Andreu, Jesús Orduna, M. Mar Ramos, and José L. Segura*

In the search of new electroactive organic dyes in dye-sensitized solar cells technology, a series of D-π-A assemblies, named as **TA-BTD-CNCOOH**, **OMeTA-BTD-CNCOOH**, **TA-Y6-CNCOOH,** and **OMeTA-Y6-CNCOOH** is rationally designed and synthesized, in which precise modifications have been carried out in order to obtain structure-performance relations in the field of dye-sensitized solar cells. After careful evaluation of the photophysical and electrochemical properties of these semiconductors, these systems are applied as active materials, showing high performance with power conversion efficiency maximum values of 9.05% and 18.5% for outdoor and indoor conditions, respectively. In addition, the best material of these organic architectures, **TA-BTD-CNCOOH**, shows an excellent long-term stability, up to 3,360 h, with no significant variance in its performance over time.

1. Introduction

On the lookout for sustainable alternatives to fossil fuels, cleaner energies are essential to mitigate climate change, reduce air pollution or greenhouse gas emissions, among others. In this regard, solar energy, harnessed from solar radiation, is one of the cleanest and most renewable sources, which is gaining importance due to its abundance, sustainability, and environmental benefits.[1] Particularly, organic-based solar technologies are in their fancy days due to their advantages in terms of flexibility, low-cost, processability, and scalability in comparison with other semiconductors.[2]

M. J. Alonso-Navarro, F. Suárez-Blas, J. L. Segura
Department of Organic Chemistry
Faculty of Chemistry
Complutense University of Madrid
28040 Madrid, Spain
E-mail: segura@ucm.es

M. J. Alonso-Navarro, F. Suárez-Blas, M. M. Ramos
Chemical and Environmental Technology department
Organic Chemistry Area
Rey Juan Carlos University
28933 Madrid, Spain

S. Franco, R. Andreu, J. Orduna
Instituto de Nanociencia y Materiales de Aragón (INMA)-Departamento de Química Orgánica
CSIC-Universidad de Zaragoza
50009 Zaragoza, Spain
E-mail: sfranco@unizar.es

Supporting information for this article is available on the WWW under https://doi.org/10.1002/cssc.202501564

In recent years, a large number of organic semiconductors have been designed, synthesized, and applied in OPV technologies. One of the most widely used electroactive materials today is the so-called Y6 (**Figure 1**), also known as BTP–4F. This semiconductor, first described in 2019,[3] presents a A_2–D–A_1–D–A_2 chemical structure with optimal photophysical, electronic, and morphological properties, which have been extensively studied to maximize its potential, reaching an impressive power conversion efficiency (PCE) of 19.06% through precise modifications.[4] As described in several research articles and reviews, many interesting approaches have been explored to achieve remarkable performance in single-junction,[5] binary,[6] or ternary[7] non-fullerene-based organic solar cells. However, from the best of our knowledge, this family of dyes has not yet been applied in other solar technologies such as dye-sensitized solar cells (DSSC).[8] Regarding the prototypical architecture of dyes in DSSC, those are composed by donor fragments, linked to a π–bridge and finally endowed with an acceptor group with the ability to be anchored to the TiO_2. In this regard, several moieties have been studied, being one of the most used donor fragments, the triphenylamine derivatives,[9] thanks to their easy functionalization and commercial availability. When evaluating the central core, two main groups have been studied over the past decades: metal-based and metal-free electroactive units. In the first group, porphyrin[10] and phthalocyanine[11] derivatives are among the most widely used semiconductors.[10,12] However, in recent years, significant efforts have been made to identify suitable metal-free organic building blocks capable of surpassing the strong performance of metal-based semiconductors. To this end, a wide range of units has been investigated, including squaraines,[13] borazines,[14] pyrazines,[15] polythiophenes,[16] benzothiadiazoles,[17] and various combinations thereof,[18] among others. However, apart from L350,[19] (Figure 1) which possesses the well-known ITIC skeleton widely used in organic solar cells (OSCs), there

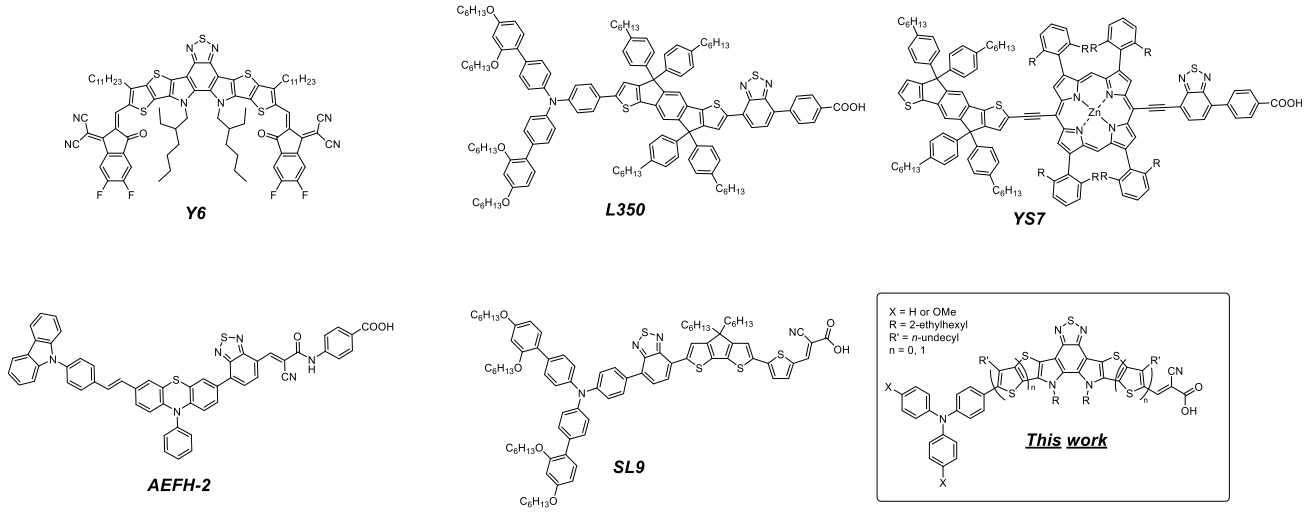

Figure 1. Chemical structures of high-performance dyes in DSSC and the general building block used in this work.

are practically no records of fully fused π-bridge structures in DSSC.[20] Finally, in the search for effective dye anchoring to TiO_2, a wide variety of functional groups have been explored to promote effective linkages,[21] with the carboxylic acid being the most commonly used moiety, along with its electron-withdrawing α–functionalized analogs.[22]

The exploration of new chemical structures in DSSC is essential to maximize key electronic processes, such as charge separation, electron transfer, and regeneration between TiO_2 and the redox electrolyte.[8a] To control these processes, fully fused polycyclic organic semiconductors represent promising candidates, mainly because 1) their planar and rigid structures enhance J_{sc} and reduces energy losses due to improved conjugation, 2) their extended π-conjugated systems broaden absorption spectra, enabling more efficient light harvesting; and 3) their processability facilitated by bulky alkyl chains or functional groups—prevents aggregation, which is crucial for maximizing photoconversion efficiency. Thus, tuning the chemical structure of organic semiconductors can be a powerful strategy to tailor their properties in line with the requirements observed in most high-performance organic sensitizers used in DSSC (Figure 1). Focusing on the Y6 block, the two main drawbacks of this high-performance building block (Y6) are: 1) the high cost of the commercially available skeleton, reaching up to 650€ g^{-1} and 2) the large number of synthetic steps for its preparation. These limitations have led the scientific community to explore simpler molecular analogs with fewer fused-ring structures, while maintaining comparable optical, electrochemical, electrical, or morphological properties.

Based on the information discussed above, in this work we designed, synthetized, and characterized four electroactive D-π-A semiconductors, named **TA-Y6-CNCOOH**, **OMeTA-Y6-CNCOOH**, **TA-BTD-CNCOOH**, and **OMeTA-BTD-CNCOOH**, specifically engineered for application in DSSC technology. This family of compound incorporates two targeted structural modifications—core-reduction and end-capping—to deepen the understanding of structure-property relationships. In this context, after careful evaluation of key DSSC parameters, the best performing fused-ring small molecule, **TA-BTD-CNCOOH**, demonstrated high efficiency under both indoor and outdoor conditions, as discussed in the following sections.

2. Results and Discussion

2.1. Synthesis and Characterization

The synthesis of the four compounds described in this work is summarized in **Scheme 1** and detailed in the electronic supporting information (ESI). Starting from the previously described D-A building blocks, **BTD** and **sY6**, the target compounds were obtained through a four steps synthetic route (all reaction conditions are provided in the ESI). First, a controlled monoformylation at one of the alpha positions of the terminal thiophene was performed via a Vilsmeier–Haack reaction, followed by a bromination of the other terminal thiophene, yielding the intermediates **Br-BTD-CHO** and **Br-Y6-CHO** in moderate to high yields. These key intermediates were then divided into two analogous synthetic routes, in which two different strong electron-donating units were introduced via Suzuki–Miyaura cross-coupling between the corresponding commercially available triarylamine (TA) boronic acids (**1** and **2**) and the brominated intermediates, yielding **TA-BTD/Y6-CHO** and **OMeTA-BTD/Y6-CHO** assemblies. Finally, a Knoevenagel-like condensation reaction between cyanoacetic acid and the corresponding aldehydes afforded the final **TA-BTD-CNCOOH**, **OMeTA-BTD-CNCOOH**, **TA-Y6-CNCOOH,** and **OMeTA-Y6-CNCOOH** compounds in good yields.

To have a deeper understanding of their chemical structure, these D-π-A assemblies have been characterized by different spectroscopic and spectrometric techniques (^1H and ^{13}C NMR, FTIR, high resolution mass spectrometry (HRMS)) and by means of thermogravimetric analysis (TGA) and diffeerential scanning

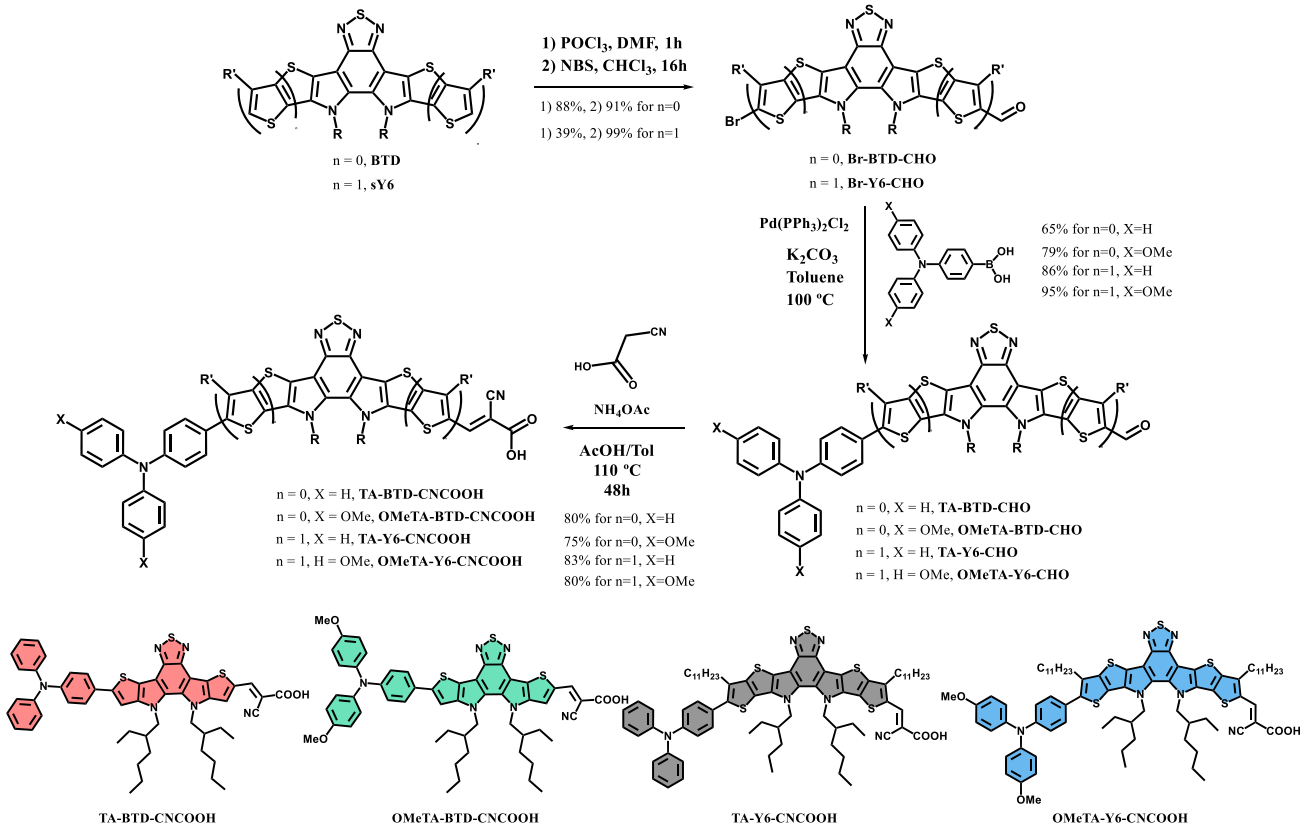

Scheme 1. Synthetic route for the preparation of the target molecules **TA-BTD-CNCOOH** (red), **OMeTA-BTD-CNCOOH** (green), **TA-Y6-CNCOOH** (grey) and **OMeTA-Y6-CNCOOH** (blue).

calorimetry (DSC). As it is shown in Figures S5, S6, S11, and S12, Supporting Information, all final compounds present the common hydrogen signal around 8.5 ppm, ascribed to the methylene unit, followed by the signals of all aromatic hydrogen atoms between 8.5–6.5 ppm, noticing the β-hydrogens of the thiophene units related to the benzothiadiazole (BTD)-based analogs around 8.25 ppm. It is also worth mentioning the two different alkyl chains of the Y6-based derivatives at 5.0–4.5 ppm and all the signals related to all different kind of aliphatic hydrogens at higher field. Regarding the ^{13}C-NMR and FTIR analysis (Figures S17, S18, S23, and S24 and S37-S40, Supporting Information), the presence of a common signal around 160 ppm (-C(O)-OEt) and a strong vibrational signal around 2200 cm^{-1} ($\nu_{C\equiv N}$) are consistent with the proper functionalization of the final compound with a strong electron-accepting cyanoacetic acid functional group. Finally, based on the high-resolution mass spectrometry analyses, we can confirm the successful synthesis of the target compounds (Figures S29, S30, S35, and S36, Supporting Information). To study the thermal properties of these novel dyes, TGA and differential scanning calorimetry measurements were carried out (Figures S41 and S42, Supporting Information) under nitrogen atmosphere. TGA only showed decomposition processes (10%) at 270–300 °C or above, temperature ranges which are suitable with fabrication requirements in organic devices. Moreover, differential scanning calorimetry results revealed no clear phase transition processes under a N_2 atmosphere in the selected range.

2.2. Theoretical Study, Optical and Electrochemical Properties

As depicted in **Figure 2**, all organic compounds exhibit similar absorption profiles, characterized by two main absorption bands: one around 365 nm, attributed to π–π* electronic transitions, and another around 553 nm, associated with an intramolecular charge transfer (ICT) process. The incorporation of 1) a more electron-donating triphenylamine unit or 2) a π-extended fused core appears to enhance the D–A character of the molecules, thereby inducing a redshift in the ICT band, as shown in Figure 2a,b. Taking this into account, the most redshifted absorption spectrum corresponds to **OMeTA-Y6-CNCOOH**, which features two methoxy groups on the triphenylamine unit and a fully fused wight-ring central core. This D–A architecture promotes high molar absorption coefficients (ε) (**Table 1**), reaching values up to 8.8×10^5 M^{-1} cm^{-1}, primarily due to the presence of fused and π-conjugated structures. This structural strategy enhances π-electron delocalization, leading to dyes with strong light-harvesting capabilities,[8a] as also reported in other studies.[23] Interestingly, the introduction of (4-(bis(4-methoxyphenyl) amino)phenyl (OMeTA) results in a decrease in the molar absorption coefficient for both BTD and Y6 derivatives, compared to their TA counterparts. Finally, regarding the length of the central core, it is observed that the larger thienopyrrole units lead to a weaker ICT band, while the π–π absorption band at 365 nm

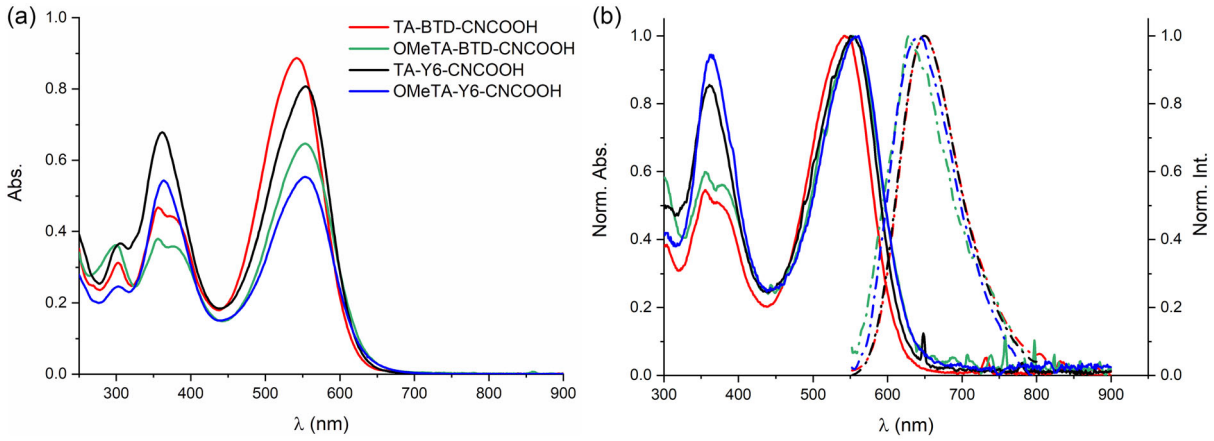

Figure 2. a) Comparison of 10^{-5} M dichloromethane solution and b) Normalized absorption (solid) and emission (dashed) spectra in dichloromethane solution for **TA-BTD-CNCOOH** (red), **OMeTA-BTD-CNCOOH** (green), **TA-Y6-CNCOOH** (black) and **OMeTA-Y6-CNCOOH** (blue).

Table 1. Physicochemical properties obtained from the UV–vis absorption measurements in dichloromethane solutions (1.0×10^{-5} M) for TA-BTD-CNCOOH, OMeTA-BTD-CNCOOH, TA-Y6-CNCOOH ,and OMeTA-Y6-CNCOOH.

	$\lambda_{abs}^{max,sol}$ [nm]	$\varepsilon_{\lambda}^{max,sol}$ [$M^{-1}\cdot cm^{-1}$]	$\lambda_{abs}^{onset,sol}$ [nm]	$\lambda_{em}^{max,sol}$ [nm]
TA-BTD-CNCOOH	544	88 000	616	651
OMeTA-BTD-CNCOOH	553	65 400	635	628
TA-Y6-CNCOOH	553	82 900	625	649
OMeTA-Y6-CNCOOH	558	55 700	635	642

Table 2. Experimental electrochemical data of the studied dyes.

	E_{ox} [a] [V]	E_{ox} [b] [V] (vs NHE)	$E_{0\text{-}0}$ [c] [eV]	E_{ox^*} [d] [V] (vs NHE)
TA-BTD-CNCOOH	+0.720	+0.919	2.074	−1.155
OMeTA-BTD-CNCOOH	+0.629	+0.828	2.083	−1.255
TA-Y6-CNCOOH	+0.740	+0.939	2.063	−1.124
OMeTA-Y6-CNCOOH	+0.644	+0.843	2.075	−1.232

[a]Oxidation potentials (E_{ox}) measured by differential pulse voltammetry (DPV) in CH_2Cl_2 with 0.1 M $TBAPF_6$ as electrolyte, using a graphite working electrode, an Ag/AgCl reference electrode, and a Pt as counter electrode. [b]E_{ox} were converted to the normal hydrogen electrode (NHE) scale by adding 0.199 V. [c]Zeroth – zeroth transition energies ($E_{0\text{-}0}$) were estimated from the wavelength corresponding to the intersection point of the normalized absorption and emission spectra. The energy values were calculated using the Planck–Einstein relation, $E = 1240\ \lambda^{-1}$. [d]Excited-state oxidation potentials (E_{ox}*) were obtained from $E_{ox} - E_{0\text{-}0}$.

becomes more pronounced, resulting in a strong and broad absorption profile across the UV–vis range.

In terms of photoluminescence, all dyes present weak fluorescent behavior, with $\lambda_{em}^{max,sol}$ around 650 nm. In addition, it is observed a blueshift in the emission maxima in solution when methoxy groups were introduced in **OMeTA-BTD-CNCOOH** and **OMeTA-Y6-CNCOOH** in comparison with the unfunctionalized **TA-BTD-CNCOOH** and **TA-Y6-CNCOOH**.

Regarding the electrochemical properties of these D–A assemblies, differential pulse voltammetry (DPV) analyses were carried out in CH_2Cl_2 solutions (**Table 2**). The voltammograms (**Figure 3**, left) were performed using 0.1 M tetrabutylammonium hexafluorophosphate as the supporting electrolyte, a glassy carbon working electrode, Ag/AgCl reference electrode and a Pt counter electrode.

The modulation of the electron-donating ability of these assemblies can be finely tuned by introducing methoxy groups into the triarylamine moiety. The electrochemical data reveal a clear trend in the first oxidation potential (E_{ox}) of the dyes: as expected, the incorporation of electron-donating substituents leads to a noticeable decrease in E_{ox}. Specifically, the values versus normal hydrogen electrode (NHE) drop from +0.919 to +0.828 V in the BTD-based series, and from +0.939 to +0.843 V for the Y6 analogs. These shifts are consistent with the increased electron density on the donor fragment, facilitating oxidation.

The optical transition energies ($E_{0\text{-}0}$) were determined from the intersection point of the normalized absorption and emission spectra in diluted dichloromethane solutions, and the excited-state oxidation pontentials (E_{ox}*) were calculated using the expresion $E_{ox}^* = E_{ox} - E_{0\text{-}0}$. All dyes exhibit E_{ox}* values significantly more negative than the conduction band edge of TiO_2 (typically around −0.5 V vs NHE),[24] ensuring thermodynamically favorable electron injection. Moreover, the ground-state E_{ox} values remain sufficiently positive relative to the redox potential of the iodide/triiodide couple (≈+0.4 V vs NHE),[25] thereby guaranteeing efficient regeneration of the oxidized dyes. (Figure 3, right).

Density functional theory (DFT) calculations were performed using the M06-2x[26]/6-311+G(2d,p)[27] model chemistry, and the most relevant optical and electrochemical parameters are gathered in **Table 3**.

Most of the calculated values are in good agreement with the experimental measurements, showing differences below 0.2 eV. The only exceptions are the ICT absorption energies, which are underestimated by ≈60 nm (0.3 eV), which is, however, a

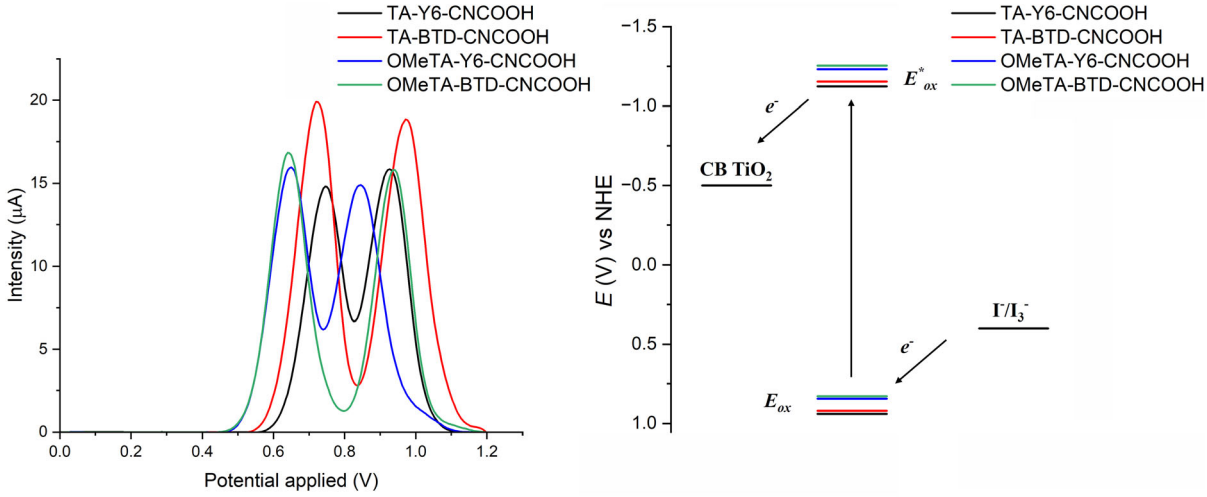

Figure 3. Left: Differential pulse voltammetry (DPV) curves of the studied dyes recorded in CH_2Cl_2 solution with 0.1 M $TBAPF_6$ as supporting electrolyte (reference electrode Ag/AgCl). Right: Energy-level diagram showing the groud-state (E_{ox}) and excited-state (E_{ox}*) oxidation potentials relative to the conduction band of TiO_2 and the redox potential of the I^-/I_3^- couple.

Table 3. Calculated optical and electrochemical parameters.

	λ_{abs} [a] [nm]	f [a,b]	λ_{em} [a] [nm]	E_{ox} [a,c] [V]	$E_{0\text{-}0}$ [a] [eV]	E_{ox^*} [a,c] [V]
TA-BTD-CNCOOH	485	2.15	613	+0.97	2.19	−1.22
OMeTA-BTD-CNCOOH	492	2.18	624	+0.81	2.17	−1.43
TA-Y6-CNCOOH	494	1.87	607	+0.98	2.24	−1.29
OMeTA-Y6-CNCOOH	496	1.87	611	+0.88	2.19	−1.37

[a]Calculated in dichloromethane using a CPCM[34] solvation model. [b]Oscillator Strength. [c]vs NHE.

reasonable result, having in mind that DFT calculations usually fail to predict charge transfer energies.[28] According to these calculations, the lowest energy absorption band corresponds to a one-electron ICT from the highest occupied molecular orbital (HOMO) located on the donor to the lowest unoccupied molecular orbital (LUMO) located on the acceptor. The absorption band observed around 365 nm arises from several overlapping transitions. The larger contribution to this band is a π–π^* transition involving a one electron promotion from the HOMO to the LUMO + 2, both located on the donor moiety (See **Figure 4** for compound **TA-Y6-CNCOOH** and Supporting Information for the rest).

Theoretical calculations predict very similar excitation energies for the four studied dyes. In good agreement to the experimental data, increasing the length of the central core in Y6 derivatives results in a small bathochromic shift and decreased oscillator strengths (f), giving rise to weaker ICT bands compared to their BTD analogs. In a similar way, the introduction of methoxy groups to the triphenylamine donor results in redshifted ICT bands.

Regarding electrochemical properties, the increased spacer length in Y6 derivatives gives rise to slightly higher oxidation potentials compared to BTD counter-pairs. Methoxy substituents increase the donor ability of triphenylamine group and give rise to higher HOMO energies and, therefore, lower oxidation potentials. It is worth noting that methoxy groups not only affect the HOMO energies but also their topology. The HOMOs of unsubstituted derivatives extend to the BTD or Y6 bridge, but those of methoxy derivatives are more localized on the donor. This effect

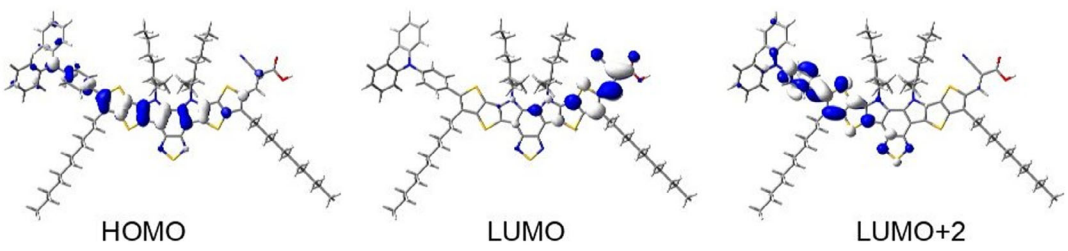

Figure 4. 0.03 contour plots of molecular orbitals involved in the lowest energy transitions of **TA-Y6-CNCOOH**.

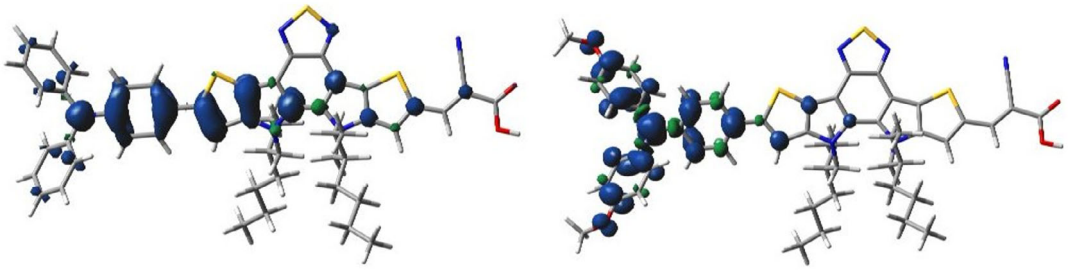

Figure 5. 0.002 contour plots of the spin density of **TA-BTD-CNCOOH**$^{+\cdot}$ (left) and **OMeTA-BTD-CNCOOH**$^{+\cdot}$ (right).

can be more clearly observed on the spin density plots of the oxidized radical cations of dyes that represent the "hole" location for these species (see **Figure 5** for BTD derivatives and Supporting Information for Y6 systems). It can be expected that molecules with a more localized HOMO give rise to a lower light absorption due to a minor HOMO–LUMO overlap but, as a counterpart, these molecules are less prone to the undesirable back electron transfer from the dye to the TiO_2 electrode.

2.3. Photovoltaic Properties of the DSSCs

DSSCs were assembled using TiO_2 photoanodes (18NR-AO) with an active area of 0.25 cm^2 and a thickness of ≈10 μm, deposited onto fluorine-doped tin oxide (FTO) glass substrates by screen-printing. The printed films were sintered and then sensitized by immersion in a 0.3 mM dye solution for 6 h. Although coadsorbents are often employed to mitigate aggregation and can enhance DSSC performance,[29] preliminary trials with chenodeoxycholic acid (CDCA) under our conditions showed no improvement; therefore, the final devices were fabricated without a coadsorbent. Platinum counter electrodes were prepared by screen-printing a Pt paste onto FTO glass, followed by thermal treatment. The electrodes were assembled using a Surlyn thermoplastic spacer, which provided both mechanical sealing and defined the electrolyte chamber. A conventional iodine-based liquid electrolyte (LPT1) was used as the redox mediator. Photovoltaic performance of the cells was evaluated under simulated sunlight at 1 sun (100 mW cm^{-2}) using a solar simulator equipped with an air mass (AM) 1.5 G filter. Measurements under low-light conditions are discussed in a separate section and additional experimental details are provided in the ESI. For each dye, three independent DSSC devices were fabricated under identical conditions, and the reported photovoltaic parameters correspond to the average values with their standard deviations (mean ± SD). Additionally, a reference device based on the benchmark sensitizer N719 was prepared under standard conditions (^{t}BuOH/acetonitrile 1:1, 18 h immersion).[30] Results are given in **Table 4**. In addition, dye-loading values were determined following the protocol described[18] and are expressed as nmol.cm^{-2}.μm^{-1}, normalized to both the film area and thickness. The current density–voltage *(J–V)* curves and incident photon-to-current conversion efficiencies (IPCE) at 1 sun are depicted in **Figure 6** and Table 4 summarizes the key photovoltaic parameters.

Among the tested dyes, **TA-BTD-CNCOOH** exhibited the best performance in the series, achieving a remarkable PCE of 9.02%, primarily attributed to its high J_{sc} and V_{oc} values, along with a moderate fill factor. Under comparable testing conditions, this PCE surpasses that of the benchmark N719 device (8.68%), highlighting the superior performance of **TA-BTD-CNCOOH**.

The notably high V_{oc} values observed suggest that the BTD molecular framework inherently suppresses dye aggregation on the TiO_2 surface, thereby enhancing photovoltage generation.

In contrast, **OMeTA-BTD-CNCOOH**, which incorporates a methoxy-substituted triphenylamine donor, exhibited a significant drop in PCE (5.24%), primarily due to a markedly lower J_{sc} and V_{oc}. This suggests that increasing the electron-donating strength of the donor unit within the BTD scaffold may raise electron density near the anchoring group, thereby enhancing the likelihood of charge recombination rates and ultimately reducing the V_{oc}.

When the π-bridge was modified from BTD to Y6, **TA-Y6-CNCOOH** exhibited a lower PCE compared to its BTD counterpart. Consistently, the dye-loading data indicate that BTD-based dyes adsorb more strongly onto the TiO_2 surface than the Y6-containing analogs. However, the introduction of a methoxy

Table 4. Photovoltaic parameters: the open circuit voltage (V_{oc}), the short circuit current (J_{sc}), the fill factor (FF), solar-to-electrical energy conversion efficiency (PCE), and lifetime (τ).

Dye	J_{sc} [mA cm^{-2}]	V_{oc} [V]	FF [%]	PCE [%]	τ [ms]	Dye loading [nmol.cm^{-2} μm^{-1}]
TA-BTD-CNCOOH	19.42 ± 0.30	0.731 ± 0.005	63.5 ± 0.7	9.02 ± 0.18	5.66	15.5
OMeTA-BTD-CNCOOH	12.50 ± 0.32	0.659 ± 0.007	63.6 ± 1.0	5.24 ± 0.18	0.59	13.5
TA-Y6-CNCOOH	14.74 ± 0.40	0.675 ± 0.006	67.8 ± 1.5	6.75 ± 0.21	3.22	7.3
OMeTA-Y6-CNCOOH	15.66 ± 0.38	0.732 ± 0.009	60.3 ± 1.3	6.91 ± 0.24	4.93	7.8
N719	15.88 ± 0.36	0.806 ± 0.006	67.8 ± 1.0	8.68 ± 0.15	–	–

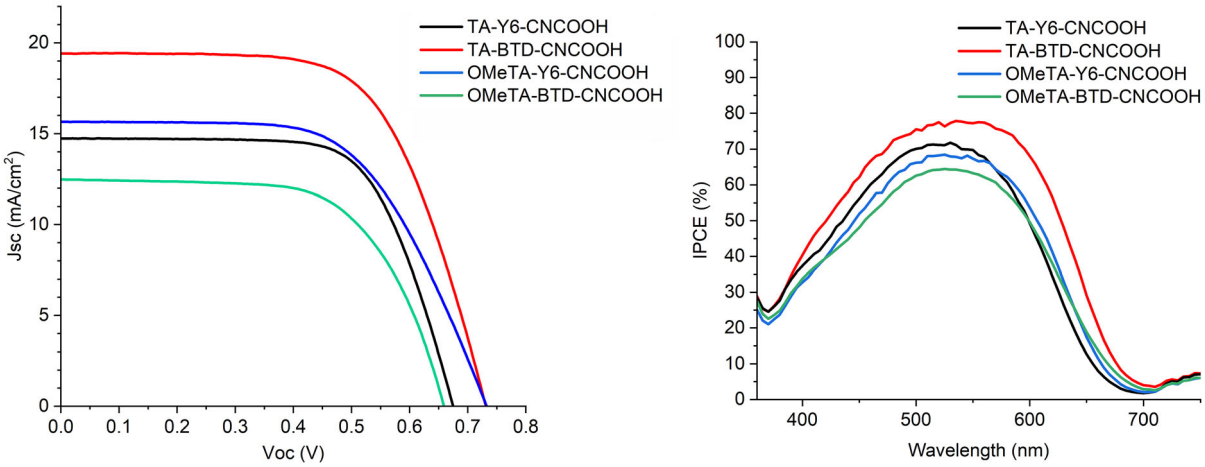

Figure 6. Current density-voltage curves (left) and IPCE spectra (right) of the DSSC based on targeted dyes.

group in **OMeTA-Y6-CNCOOH** resulted in a slight improvement in efficiency (PCE = 6.91%). This trend suggests that the electronic characteristics of the Y6 unit are more compatible with the methoxy-substituent donor, partially mitigating the performance losses observed in the BTD-based analog. Overall, the observed differences highlight the importance of the interplay between donor strength and π-bridge identity in modulating both charge separation efficiency and recombination dynamics in these D-π-A systems.

The IPCE spectra (Figure 6-right) further support these observations, exhibiting broad response curves in the 400–690 nm range, indicating efficient photon-to-electron conversion across the visible spectrum. The maxima, observed between 500–560 nm, align with the absorption characteristics of the dyes and suggest effective light harvesting in this region. Furthermore, the integrated IPCE values correlate well with the measured J_{sc}, confirming the reliability of the photovoltaic performance data.

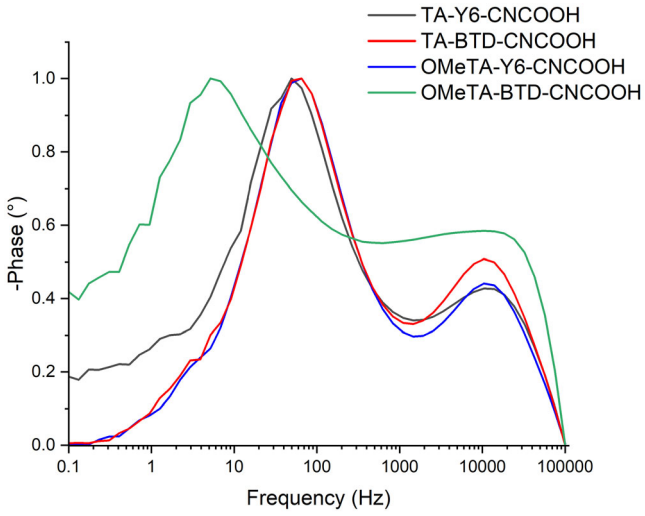

Figure 7. Normalized Bode plots of DSSC measured under open-circuit conditions.

3. Electrochemical Impedance Spectroscopy Analysis (EIS)

Electrochemical impedance pectroscopy (EIS)[31] is commonly used to investigate the internal processes of DSSC, particularly those related to charge transport and interfacial recombination. Among the various representations, Bode plots are especially useful for identifying the characteristic timescales of these processes. In particular, the electron lifetime (τ) can be estimated from the frequency (f_{max}) at which the phase reaches its maximum, using the expression

$$\tau = \frac{1}{2\pi f_{max}} \quad (1)$$

This lifetime reflects the average time that photogenerated electrons remain in the semiconductor before recombining. Since longer lifetimes are generally associated with reduced recombination losses, they tend to correlate with higher V_{oc}, as the quasi-Fermi level of electrons shifts closer to the conduction band edge. In the present study, the characteristic frequencies were extracted from normalized Bode phase plots (**Figure 7**), and the calculated lifetimes showed a consistent trend with the measured V_{oc} values. Devices based on **OMeTA-Y6-CNCOOH** and **TA-BTD-CNCOOH** exhibited similar and relatively long lifetimes (4.93 and 5.66 ms, respectively), corresponding to the highest V_{oc} values (0.732 V) and suggesting efficient suppression of recombination. Conversely, the DSSC based on **OMeTA-BTD-CNCOOH** showed a significantly shorter electron lifetime (0.59 ms), however, its V_{oc} (0.659 V) was only moderately lower. This behavior reflects the nonlinear nature of the relationship between carrier lifetime and photovoltage. It also indicates that, in addition to recombination dynamics, other factors such as injection efficiency or interfacial quality may contribute to the overall V_{oc} outcome.

This behavior has not been observed in dyes incorporating the Y6 spacer, which shows a slight increase in PCE values in

molecules containing methoxy groups, as has been consistently reported in other dye series.[32]

3.1. DSC Performance under Indoor-Light Conditions

Among the most promising applications of DSSC is their integration in low-power electronics operating under ambient or indoor conditions. Unlike conventional photovoltaics, DSSC exhibit superior spectral matching with artificial light sources and retain high performance under low-irradiance environments.[33]

To investigate the performance of the dyes under artificial light conditions, DSSC devices similar to those described in the previous section were fabricated. As a benchmark, a reference device sensitized with N719 was also measured under the same indoor conditions. An 18 W OSRAM 930 fluorescent tube (commonly employed in indoor photovoltaic studies) was used as the light source (its emission spectrum is provided in Figure S55, Supporting Information). Measurements were carried out at illuminance levels of 1000 and 3500 lux. The light source was calibrated to establish the relationship between illuminance (lux) and irradiance (watts per square meter). As a reference, 1000 lux corresponds to ≈1% of the irradiance under 1 sun (100 mW cm^{-2}). The PCE values under indoor conditions were calculated using the following expression

$$\mathrm{PCE} = \frac{P_{out}}{P_{in}} \times 100$$

where P_{out} is the output power of the solar cell and P_{in} is the incident power of the fluorescent source, estimated from lux measurements using a calibrated lux meter. In general, higher PCE values are expected under indoor lighting compared to simulated sunlight, since artificial light sources primarily emit within the visible range (380–750 nm), which matches well with the absorption spectra of most organic dyes. Data are shown in **Figure 8** and **Table 5**.

The results obtained show that at both 1000 and 3400 lux, the PCE values were comparable. It is worth noting that the fill factor (FF) values improved significantly due to a combination of factors such as the lower light intensity, the narrower spectrum, the reduction in recombination processes, and the lower thermal stress resulting from reduced heat generation, which overall ensures more stable operating conditions.

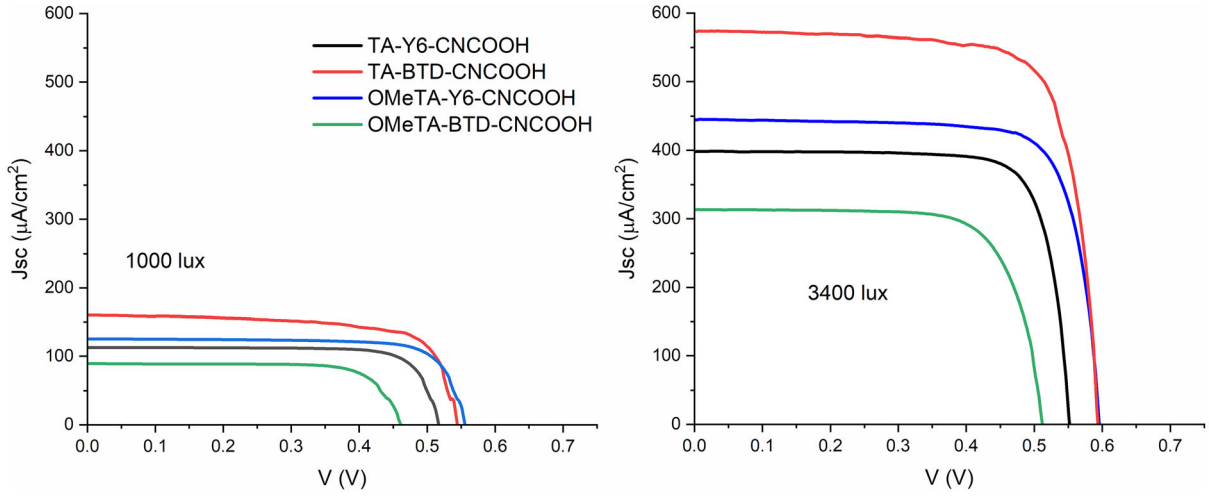

Figure 8. The Current density-voltage curves of the DSSC measured at 1000 lux (left) and 3400 lux (right).

Table 5. Photovoltaic data for DSSC under indoor light conditions (OSRAM 930) at 1000 and 3400 lux.

Dye	[lux]	J_{sc} [μA cm^{-2}]	V_{oc} [V]	FF [%]	P_{in} [μW cm^{-2}]	P_{out} [μW cm^{-2}]	PCE [%]
TA-BTD-CNCOOH	1000	160	0.544	71.8	366.1	62.5	17.1
	3400	575	0.594	75.7	1398.1	258.6	18.5
OMeTA-BTD-CNCOOH	1000	89	0.460	78.8	366.1	31.0	8.5
	3400	313	0.512	73.2	1398.1	117.3	8.4
TA-Y6-CNCOOH	1000	113	0.517	78.8	366.1	46.0	12.6
	3400	399	0.552	78.7	1398.1	173.3	12.4
OMeTA-Y6-CNCOOH	1000	125	0.555	77.7	366.1	53.9	14.7
	3400	445	0.596	77.5	1398.1	205.5	14.7
N719	1000	127	0.640	69.6	366.1	56.7	15.5
–	3400	439	0.690	78.7	1398.1	238.4	17.1

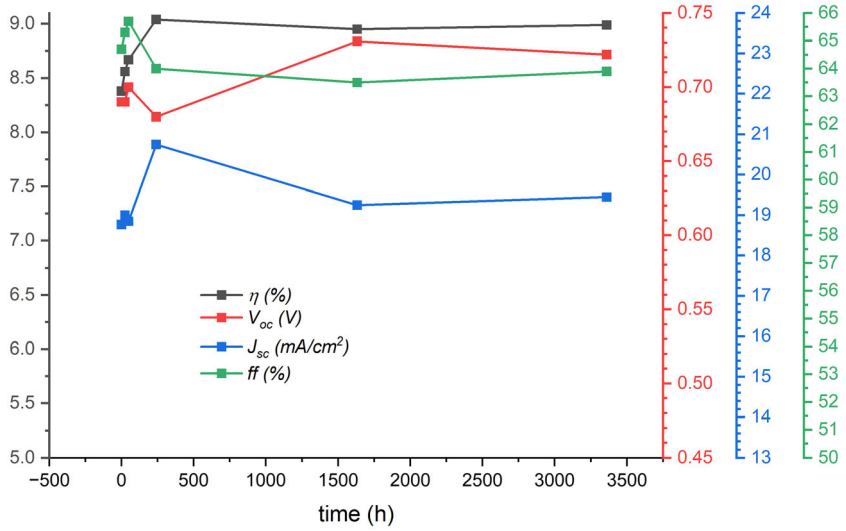

Figure 9. Temporal evolution of the photovoltaic parameters of devices prepared with dye **TA-BTD-CNCOOH**. Measurements were performed under AM 1.5 G simulated solar light (1 sun 1000 W m^{-2}).

Notably, the **TA-BTD-CNCOOH** dye stood out with a PCE of 18.5% at 3400 lux. For comparison, the benchmark N719 yielded 15.5% and 17.1% at 1000 and 3400 lux (data annexed in the ESI). This is a highly competitive value that could enable its use in internet of things (IoT) devices as an alternative to conventional batteries, since the power consumption required for these devices can be achieved with DSSC under indoor lighting conditions.

The DSSC devices incorporating dye **TA-BTD-CNCOOH** exhibited exceptional long-term stability, with an initial increase in efficiency during the first three days. This behavior is commonly observed in DSSCs with bulky dye molecules and is likely due to the time required for the electrolyte to fully infiltrate the mesoporous TiO_2 photoanode, optimizing the dye-electrolyte interface and charge transfer dynamics. Following this initial enhancement, the efficiency, measured under continuous 1 sun illumination, remained nearly constant for at least 3,360 h, with no significant signs of degradation. The long-term evolution of key photovoltaic parameters is presented in **Figure 9**.

4. Conclusion

To sum up, we have designed and synthesized a family of D-π-A dyes based on fully fused central core structures, endowed with both strong electron-donating units and a carboxylic group to be anchored to TiO_2 for DSSC technologies. The precise functionalization with different triarylamines as well as the control over the length of the fused central core allow us to rationally manipulate their optical and electrochemical properties of the dyes, modulating their frontier orbital energy levels, results which are in good agreement with the theoretical calculations carried out. The DSSC employing **TA-BTD-CNCOOH** as active material and using I^-/I_3^- as redox shuttle recorded the best performance of the family, with a maximum PCE value of 9.02% under outdoor conditions. This performance can be rationalized, not only in terms of its chemical structure, but also in terms of its high J_{sc} and V_{oc} values, along with a moderate fill factor and relatively long lifetimes, suggesting efficient suppression of recombination processes. Finally, all the dyes studied in this work have been employed in indoor DSSC, where **TA-BTD-CNCOOH** dye showed a PCE of 18.5% at 3400 lux and exhibited exceptional long-term stability, with an initial increase in efficiency during the first three days and remained nearly constant for at least 3,360 h.

Supporting Information

The authors have cited additional references within the Supporting Information.[3,27–28,35]

Acknowledgements

This work was financially supported by the MICINN (PID2022-138908NB-C33, TED2021-129886BC43, RED2022-134503-T and Grant CEX2023-001286-S funded by MICIU/AEI /10.13039/501100011033), Comunidad de Madrid (TEC-2024/ECO-332), Gobierno de Aragón (E47_23R), the University of Zaragoza (UZ2023-CIE01), the UCM (INV.GR.00.1819.10759) and the URJC ((2024/SOLCON-138169). M.J.A.-N. and F.S.-B. gratefully acknowledge Universidad Rey Juan Carlos for his postdoctoral contract and her predoctoral contract respectively.

Conflict of Interest

The authors declare no conflict of interest.

Data Availability Statement

The data that support the findings of this study are available from the corresponding author upon reasonable request.

Keywords: dye-sensitized solar cells · fully fused semiconductors · indoor-outdoor performances · metal-free assemblies · organic photovoltaics

[1] a) F. J. M. M. Nijsse, J.-F. Mercure, N. Ameli, F. Larosa, S. Kothari, J. Rickman, P. Vercoulen, H. Pollitt, *Nat. Commun.* **2023**, *14*, 6542; b) A. Kumler, B. Kravitz, C. Draxl, L. Vimmerstedt, B. Benton, J. K. Lundquist, M. Martin, H. J. Buck, H. Wang, C. Lennard, L. Tao, *Renew. Sustain. Energy Rev.* **2025**, *207*, 114934.
[2] a) T. Kirchartz, G. Yan, Y. Yuan, B. K. Patel, D. Cahen, P. K. Nayak, *Nat. Rev. Mater.* **2025**, *10*, 335; b) Y.-C. Tseng, L.-H. Yeh, H.-L. Yip, C.-C. Chueh, *Small* **2025**, *21*, 2412507.
[3] J. Yuan, Y. Zhang, L. Zhou, G. Zhang, H.-L. Yip, T.-K. Lau, X. Lu, C. Zhu, H. Peng, P. A. Johnson, M. Leclerc, Y. Cao, J. Ulanski, Y. Li, Y. Zou, *Joule* **2019**, *3*, 1140.
[4] J. Luo, W. Zhou, Y. Li, C. Liao, X. Xu, Q. Peng, *Adv. Funct. Mater.* **2025**, *35*, 2501851.
[5] L. Zhu, M. Zhang, J. Xu, C. Li, J. Yan, G. Zhou, W. Zhong, T. Hao, J. Song, X. Xue, Z. Zhou, R. Zeng, H. Zhu, C.-C. Chen, R. C. I. MacKenzie, Y. Zou, J. Nelson, Y. Zhang, Y. Sun, F. Liu, *Nat. Mater.* **2022**, *21*, 656.
[6] J. Fu, P. W. K. Fong, H. Liu, C.-S. Huang, X. Lu, S. Lu, M. Abdelsamie, T. Kodalle, C. M. Sutter-Fella, Y. Yang, G. Li, *Nat. Commun.* **2023**, *14*, 1760.
[7] J. Zhang, A. Liang, C. Zhu, S. Huang, S. Chung, H. Ji, J. Shin, K. Cho, L. Li, Z. Kan, *J. Mater. Chem. C* **2025**, *13*, 8494.
[8] a) H. Zhou, M. Aftabuzzaman, Masud, S. H. Kang, H. K. Kim, *ACS Energy Lett.* **2025**, *10*, 881; b) X.-L. Wang, J.-F. Huang, J.-M. Liu, P. Tsiakaras, *Coord. Chem. Rev.* **2025**, *522*, 216143; c) A. Sen, M. H. Putra, A. K. Biswas, A. K. Behera, A. Groβ, *Dyes Pigm.* **2023**, *213*, 111087.
[9] E. Elbashier, P. Wagner, D. L. Officer, K. C. Gordon, *J. Phys. Chem. A* **2025**, *129*, 1026.
[10] F. A. Faraghally, Y.-H. Chen, T.-Z. Lee, Y.-D. Chen, T.-C. Wei, C.-Y. Yeh, *Sustain. Energy Fuels* **2025**, *9*, 2369.
[11] Ş. N. Süerkan, N. Arslan, A. T. Gökçeören, S. Çakar, A. M. Sevim, A. Gül, M. Özacar, *J. Photochem. Photobiol. A: Chem.* **2025**, *464*, 116333.
[12] R. Milan, G. S. Selopal, M. Cavazzini, S. Orlandi, R. Boaretto, S. Caramori, I. Concina, G. Pozzi, *Sci. Rep.* **2017**, *7*, 15675.
[13] J. Alkabli, Y. Q. Almulaiky, S. A. Al-horaibi, *Appl. Mater. Today* **2025**, *42*, 102590.
[14] S. Chowdhury, V. C. Wakchure, E. C. Galleposo, D. Bonifazi, R. D. Costa, *Adv. Energy Sustain. Res.* **2025**, *6*, 2400344.
[15] X. Zhang, J. Mao, D. Wang, X. Li, J. Yang, Z. Shen, W. Wu, J. Li, H. Ågren, J. Hua, *ACS Appl. Mater. Interfaces* **2015**, *7*, 2760.
[16] D. M. Almenningen, H. E. Hansen, A. F. Buene, B. H. Hoff, O. R. Gautun, *Dyes Pigm.* **2022**, *207*, 110700.
[17] Y. Farré, M. Raissi, A. Fihey, Y. Pellegrin, E. Blart, D. Jacquemin, F. Odobel, *Dyes Pigm.* **2018**, *148*, 154.
[18] Y. Ren, D. Zhang, J. Suo, Y. Cao, F. T. Eickemeyer, N. Vlachopoulos, S. M. Zakeeruddin, A. Hagfeldt, M. Grätzel, *Nature* **2023**, *613*, 60.
[19] Y. Liu, Y. Cao, W. Zhang, M. Stojanovic, M. I. Dar, P. Péchy, Y. Saygili, A. Hagfeldt, S. M. Zakeeruddin, M. Grätzel, *Angew. Chem. Int. Ed.* **2018**, *57*, 14125.
[20] Z.-S. Huang, H.-L. Feng, X.-F. Zang, Z. Iqbal, H. Zeng, D.-B. Kuang, L. Wang, H. Meier, D. Cao, *J. Mater. Chem. A* **2014**, *2*, 15365.
[21] a) A. Bartkowiak, O. Korolevych, B. Gierczyk, D. Pelczarski, A. Bossi, M. Klein, Ł. Popenda, W. Stampor, M. Makowska-Janusik, M. Zalas, *Sci. Rep.* **2023**, *13*, 16808; b) S. J. Sharma, J. Prasad, S. S. Soni, N. Sekar, *J. Photochem. Photobiol. A: Chem.* **2023**, *444*, 114915; c) L. Zhang, J. M. Cole, *ACS Appl. Mater. Interfaces* **2015**, *7*, 3427.
[22] C. C. Syiemlieh, B. Ilango, R. Kothandaraman, P. Venkatakrishnan, M. Velusamy, A. Kathiravan, *J. Phys. Chem. C* **2025**, *129*, 5821.
[23] S. H. Kim, J. Choi, C. Sakong, J. W. Namgoong, W. Lee, D. H. Kim, B. Kim, M. J. Ko, J. P. Kim, *Dyes Pigm.* **2015**, *113*, 390.
[24] M. Grätzel, *Nature* **2001**, *414*, 338.
[25] H. Tian, L. Sun, *J. Mater. Chem.* **2011**, *21*, 10592.
[26] Y. Zhao, D. G. Truhlar, *Theor. Chem. Acc.* **2008**, *120*, 215.
[27] P. C. Hariharan, J. A. Pople, *Theor. Chim. Acta* **1973**, *28*, 213.
[28] S. Kümmel, *Adv. Energy Mater.* **2017**, *7*, 1700440.
[29] J.-S. Ni, Y.-C. Yen, J. T. Lin, *Chem. Commun.* **2015**, *51*, 17080.
[30] P. J. Holliman, M. L. Davies, A. Connell, B. V. Velasco, T. M. Watson, *Chem. Commun.* **2010**, *46*, 7256.
[31] Q. Wang, J.-E. Moser, M. Grätzel, *J. Phys. Chem. B* **2005**, *109*, 14945.
[32] J. Wang, K. Liu, L. Ma, X. Zhan, *Chem. Rev.* **2016**, *116*, 14675.
[33] H. Michaels, M. Rinderle, I. Benesperi, R. Freitag, A. Gagliardi, M. Freitag, *Chem. Sci.* **2023**, *14*, 5350.
[34] a) V. Barone, M. Cossi, *J. Phys. Chem. A* **1998**, *102*, 1995; b) M. Cossi, N. Rega, G. Scalmani, V. Barone, *J. Comput. Chem.* **2003**, *24*, 669.
[35] a) R. González-Núñez, M. J. Alonso-Navarro, F. Suárez-Blas, E. Gala, M. M. Ramos, J. L. Segura, R. Ponce Ortiz, *Mater. Chem. Front.* **2024**, *8*, 1981; b) H. S. Kim, J. B. Park, J.-H. Kim, D.-H. Hwang, *J. Nanosci. Nanotechnol.* **2015**, *15*, 8876; c) J. Yuan, Y. Zhang, L. Zhou, C. Zhang, T.-K. Lau, G. Zhang, X. Lu, H.-L. Yip, S. K. So, S. Beaupré, M. Mainville, P. A. Johnson, M. Leclerc, H. Chen, H. Peng, Y. Li, Y. Zou, *Adv. Mater.* **2019**, *31*, 1807577; d) Gaussian 16, Revision C.01, M. J. Frisch, G. W. Trucks, H. B. Schlegel, G. E. Scuseria, M. A. Robb, J. R. Cheeseman, G. Scalmani, V. Barone, G. A. Petersson, H. Nakatsuji, X. Li, M. Caricato, A. V. Marenich, J. Bloino, B. G. Janesko, R. Gomperts, B. Mennucci, H. P. Hratchian, J. V. Ortiz, A. F. Izmaylov, J. L. Sonnenberg, D. Williams-Young, F. Ding, F. Lipparini, F. Egidi, J. Goings, B. Peng, A. Petrone, T. Henderson, et al., Gaussian, Inc., Wallingford CT **2016**.

Manuscript received: July 18, 2025
Revised manuscript received: September 5, 2025
Version of record online: